nature COMMUNICATIONS

ARTICLE

Received 26 Jun 2013 | Accepted 17 Mar 2014 | Published 14 Apr 2014

DOI: 10.1038/ncomms4663

Mechanisms of charge transfer and redistribution in $LaAlO_3/SrTiO_3$ revealed by high-energy optical conductivity

T.C. Asmara[1,2,3], A. Annadi[1,2], I. Santoso[1,2,3], P.K. Gogoi[1,2,3], A. Kotlov[4], H.M. Omer[3], M. Motapothula[1,2,5], M.B.H. Breese[2,3,5], M. Rübhausen[1,6,7], T. Venkatesan[1,2,8], Ariando[1,2] & A. Rusydi[1,2,3]

In condensed matter physics the quasi two-dimensional electron gas at the interface of two different insulators, polar $LaAlO_3$ on nonpolar $SrTiO_3$ ($LaAlO_3/SrTiO_3$) is a spectacular and surprising observation. This phenomenon is $LaAlO_3$ film thickness dependent and may be explained by the polarization catastrophe model, in which a charge transfer of $0.5e^-$ from the $LaAlO_3$ film into the $LaAlO_3/SrTiO_3$ interface is expected. Here we show that in conducting samples ($\geq$4 unit cells of $LaAlO_3$) there is indeed a $\sim 0.5e^-$ transfer from $LaAlO_3$ into the $LaAlO_3/SrTiO_3$ interface by studying the optical conductivity in a broad energy range (0.5–35 eV). Surprisingly, in insulating samples ($\leq$3 unit cells of $LaAlO_3$) a redistribution of charges within the polar $LaAlO_3$ sublayers (from AlO_2 to LaO) as large as $\sim 0.5e^-$ is observed, with no charge transfer into the interface. Hence, our results reveal the different mechanisms for the polarization catastrophe compensation in insulating and conducting $LaAlO_3/SrTiO_3$ interfaces.

[1] NUSNNI-NanoCore, National University of Singapore, Singapore 117411, Singapore. [2] Department of Physics, National University of Singapore, Singapore 117576, Singapore. [3] Singapore Synchrotron Light Source, National University of Singapore, Singapore 117603, Singapore. [4] Hamburger Synchrotronstrahlungslabor (HASYLAB) at Deutsches Elektronen-Synchrotron (DESY), Notkestrasse 85, 22603 Hamburg, Germany. [5] Department of Physics, Center for Ion Beam Applications (CIBA), National University of Singapore, Singapore 117542, Singapore. [6] Institut für Angewandte Physik, Universität Hamburg, Jungiusstrasse 11, D-20355 Hamburg, Germany. [7] Center for Free Electron Laser Science (CFEL), Notkesstrasse 85, D-22607 Hamburg, Germany. [8] Department of Electrical and Computer Engineering, National University of Singapore, Singapore 117583, Singapore. Correspondence and requests for materials should be addressed to A.R. (email: phyandri@nus.edu.sg).

Some of the most exciting condensed matter physics problems are found at the interfaces of dissimilar materials[1]. The behaviour of electrons at these interfaces would be governed by electronic reconstruction mechanisms[2] leading to a variety of exotic quantum phenomena[1]. In conjunction with X-ray and electron spectroscopy techniques[3–7] with their inherent advantages and constraints, an experimental technique that can directly reveal hidden quantum phenomena at buried interfaces is highly desirable. In this paper we demonstrate the potency of high-energy optical reflectivity coupled with spectroscopic ellipsometry and study an interface consisting of two dissimilar insulators: polar $LaAlO_3$ and nonpolar $SrTiO_3$ revealing the details of the charge (electron) transfer among and within the layers that govern the conductivity of the buried interface.

The quasi two-dimensional electron gas (2DEG) at the the buried interface of two different insulator oxides heterostructure, polar $LaAlO_3$ on nonpolar $SrTiO_3$ ($LaAlO_3/SrTiO_3$)[8] has shown many interesting phenomena ranging from metal–insulator transition[9], superconductivity[10] and magnetism[11–14]. According to the controversial but compelling polarization catastrophe model, the polar sublayers of $LaAlO_3$ ($(LaO)^+$ and $(AlO_2)^-$) give rise to a polarization field inside $LaAlO_3$ that causes an electronic potential build-up as the $LaAlO_3$ film thickness increases. To counter this, a charge transfer of $0.5e^-$ per unit cell (uc) ($\sim 3\times10^{14}\,cm^{-2}$) from $LaAlO_3$ into the $LaAlO_3/SrTiO_3$ interface is required[15,16]. Various techniques have shown a charge transfer much less than this. For example, X-ray-based techniques[5,6] have estimated up to $1.1\times10^{14}\,cm^{-2}$ while transport measurements[9–11] yield substantially smaller number of carriers of $\sim10^{13}\,cm^{-2}$. It has been suggested that charge localization effects might limit the number of mobile charges that can be measured by transport[7,17], and thus if a technique can measure and quantify both the localized and delocalized charges, one might be able to evaluate the actual charge transfer[5–7].

Another unresolved important issue is the insulating case of $LaAlO_3/SrTiO_3$ ($\leq$3 uc of $LaAlO_3$). Transport measurements[9] have shown that the conducting interface only exists above a certain critical thickness of $LaAlO_3$, typically $\geq$4 uc (although cationic stoichiometry, for example the La/Al ratio of $LaAlO_3$ film, may also affect the interface conductivity, with conducting $LaAlO_3/SrTiO_3$ observed to have slightly Al-rich $LaAlO_3$ film[18]). This means that the charge transfer into the interface required for countering the polarization catastrophe does not happen when the thickness of $LaAlO_3$ is below 4 uc. According to the prevalent polarization catastrophe model, this means the polarization field should be present for $\leq$3 uc of $LaAlO_3$. One way to verify the model is to measure this polarization potential build-up in insulating $LaAlO_3/SrTiO_3$, which is predicted to be $0.24\,V\,Å^{-1}$ (or ~0.9 V per uc of $LaAlO_3$)[19]. However, attempts to measure this have not been successful using core-level X-ray photoemission spectroscopy (XPS)[20,21], in which the measured core-level shift in $LaAlO_3$ is only ~0.1 eV per uc of $LaAlO_3$, much less than expected. If the changes in the band structure are predominantly near the valence bands and the Fermi level, then the appropriate technique should directly probe states near the valence bands and the Fermi level.

Let us approach the problem from a different angle. Another way to overcome the polarization potential is by charge redistribution within the $LaAlO_3$ layers. In a *Gedankenexperiment*, we hypothesize an extreme case of charge redistribution of $1e^-$ between the AlO_2 and LaO sublayers of $LaAlO_3$, which is also adequate to compensate the polarization potential, although the actual amount of charge redistribution might be restricted by electrostatics. Hence, instead of measuring the potential build-up in the layers, one can measure the charge redistribution within the layers directly. This can be done by measuring the optical conductivity involving states below and above the valence bands, the conduction bands and the Fermi level, and then use the f-sum rule, which represents charge conservation, to quantify the charge redistribution.

Furthermore, recent band structure calculations and surface X-ray diffraction measurements suggest that distortions of the $LaAlO_3$ lattice (buckling) may partly compensate the polarization field in insulating $LaAlO_3/SrTiO_3$ (refs 22–25). Interestingly, when the interface becomes conducting at $LaAlO_3$ thickness $\geq$4 uc, this distortion decreases and ultimately vanishes[24,25], indicating that the buckling mechanism is unique to the insulating case of $LaAlO_3/SrTiO_3$. This raises another important question: since the buckling is a structural change, will the electronic structure change appropriately, and manifest as a charge redistribution within the $LaAlO_3$ layer itself? Thus, it is again critical to be able to measure these intralayer charge redistributions.

As mentioned earlier, a direct way to probe the electronic band structure and charge (localized and delocalized) redistribution mechanisms is to measure the complex dielectric response of the material from which the optical conductivity can be extracted in a broad energy range[26–28]. Here we use a combination of spectroscopic ellipsometry and ultraviolet–vacuum ultraviolet (UV-VUV) reflectivity to probe the intrinsic properties of the $LaAlO_3/SrTiO_3$ interface using photon with energies between 0.5 and 35 eV. Owing to a stabilized Kramers–Kronig transformation[29,30], the strength of this experimental approach allows one to measure the charge transfer of both delocalized and localized charges accurately using the optical f-sum rule. Since localized electrons are inaccessible to electrical transport measurements, but are accessible by photons, we overcome a severe constraint. In particular, the optical transitions involving AlO_2 sublayer of $LaAlO_3$ is very distinct and well separated from the ones involving LaO sublayer, so that the internal charge redistribution within the $LaAlO_3$ sublayers can be clearly identified. The same is also true for the TiO_2 and SrO sublayers of $SrTiO_3$.

Here we show that in conducting $LaAlO_3/SrTiO_3$ (4 and 6 uc of $LaAlO_3$ film on $SrTiO_3$), there is indeed a charge transfer from $LaAlO_3$ into the interface, and that the amount of charge transfer is $\sim0.5e^-$. In the insulating case (2 and 3 uc of $LaAlO_3$ film on $SrTiO_3$), we surprisingly observe $\sim0.5e^-$ charge redistribution from AlO_2 to LaO sublayers, within the $LaAlO_3$ layers. This suggests that for the insulating case the polarization catastrophe could be partly overcome by the above-mentioned charge redistribution, which may be a consequence of the buckling of the $LaAlO_3$ lattice.

Results

Structural and transport measurements. $LaAlO_3/SrTiO_3$ samples were prepared by growing $LaAlO_3$ film on top of TiO_2-terminated (001) $SrTiO_3$ using pulsed laser deposition[12]. The atomic force microscopy (AFM) topography image of the TiO_2-terminated $SrTiO_3$ substrate in Fig. 1a clearly shows the atomically flat surface with uc steps. Four high-quality samples with varying thickness of 2, 3, 4 and 6 uc of $LaAlO_3$ film were prepared as a model interface system for the high-energy optical studies. The growth of the films was monitored using reflective high-energy electron diffraction (Fig. 1b). After $LaAlO_3$ deposition, AFM topography measurements show that the atomically flat surface with uc step and terrace structure of $SrTiO_3$ is preserved, with surface roughness of ~1 Å (see Fig. 1c,d). This ensures that surface roughness effects do not adversely affect the optical measurements. Transport measurements (Fig. 1e), which were taken before and after the

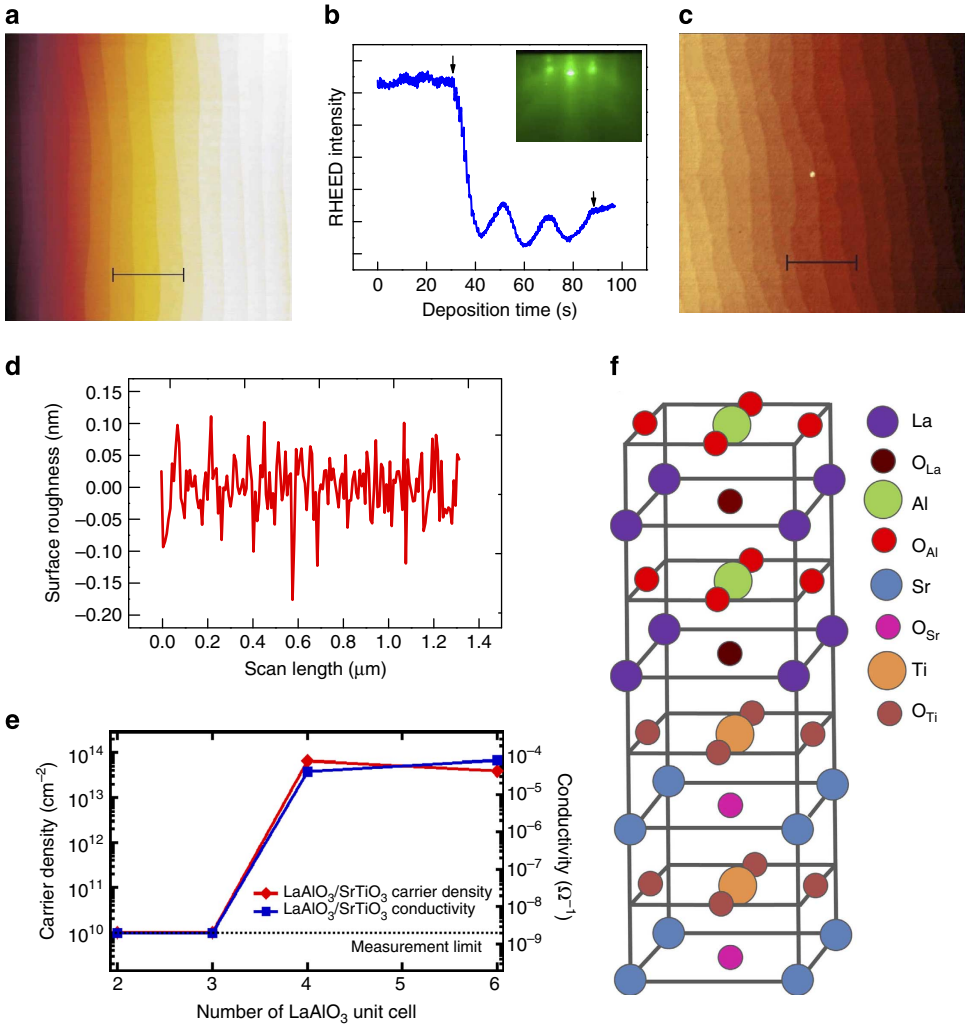

Figure 1 | Characterization results and crystal structure of $LaAlO_3/SrTiO_3$. (**a**) AFM topography image of TiO_2-terminated $SrTiO_3$ substrate. Scale bar, 1 μm. (**b**) Reflective high-energy electron diffraction (RHEED) oscillations obtained for growth of 3 unit cells (uc) of $LaAlO_3$ film on $SrTiO_3$ substrate; inset shows obtained RHEED pattern after the $LaAlO_3$ growth. (**c**) AFM topography image of 4 uc $LaAlO_3/SrTiO_3$, showing the preserved atomically smooth surface. Scale bar, 1 μm. (**d**) The surface roughness of 4 uc $LaAlO_3/SrTiO_3$ as extracted from the AFM data, measured to be ~1 Å. For other $LaAlO_3/SrTiO_3$ samples (2, 3 and 6 uc $LaAlO_3/SrTiO_3$), the roughness variation and the surface AFM images are found to not alter very much as the $LaAlO_3$ thickness is below 15 uc and the layer-by-layer growth mode is preserved. (**e**) Electrical transport data of the $LaAlO_3/SrTiO_3$ samples as a function of $LaAlO_3$ film thickness. (**f**) Crystal structure of $LaAlO_3/SrTiO_3$.

optics measurements, show consistently that 2 and 3 uc samples are insulating with carrier density and conductivity below the measurement limit, while 4 and 6 uc ones are conducting with carrier density of $4–6 \times 10^{13}\,cm^{-2}$ and conductivity of $4–8 \times 10^{-5}\,\Omega^{-1}$, consistent with previous transport results[9–11].

The perovskite $LaAlO_3$ uc (Fig. 1f) can be divided into two sublayers: LaO and AlO_2, in which theoretical calculations have shown that the band structures of these discriminated sublayers are indeed different[19,22], leading to distinct optical transitions. To accommodate the assignments of these optical transitions, we define O_{La} as the O in the LaO plane and O_{Al} as the O in the AlO_2 plane. Similarly, $SrTiO_3$ also has similar layered perovskite structure and thus can also be divided into two sublayers: SrO and TiO_2. Then O_{Sr} is defined as O that belongs to SrO sublayer, while O_{Ti} is defined as the one in TiO_2. Similarly, the O in the different planes of $SrTiO_3$ can also lead to distinct optical transitions. This discrimination is important, as discussed later, because it can reveal the intra- and interlayer charge transfer mechanism in $LaAlO_3/SrTiO_3$ for both the insulating and conducting samples.

Spectroscopic ellipsometry and high-energy reflectivity. Our main observation is the high-energy reflectivity of $LaAlO_3/SrTiO_3$ at different thicknesses of $LaAlO_3$ as compared with bulk $LaAlO_3$ and $SrTiO_3$ as shown in Fig. 2a. Note that, because of the challenge in making optical measurements over such a broad energy range, in this study we have only measured a selected set of samples as representative of insulating (2 and 3 uc) and conducting (4 and 6 uc) $LaAlO_3/SrTiO_3$. Thus, further measurements on a larger set of samples may be important in further deepening our analyses. It can be seen that the reflectivity spectra of the insulating 2 and 3 uc $LaAlO_3/SrTiO_3$ are similar, and the same is true for the conducting 4 and 6 uc $LaAlO_3/SrTiO_3$. Surprisingly, there are huge differences between reflectivity of insulating and conducting samples. These differences occur more significantly at high photon energies, particularly in the energy ranges of 9–14 eV and 14–21 eV. In the 9–14-eV range, the reflectivity of conducting samples is lower than insulating samples, while in the 14–21-eV range the opposite occurs. In contrast, between 4 and 9 eV, the differences are less, and below 4 eV they are negligible. This signifies why going beyond conventional (up

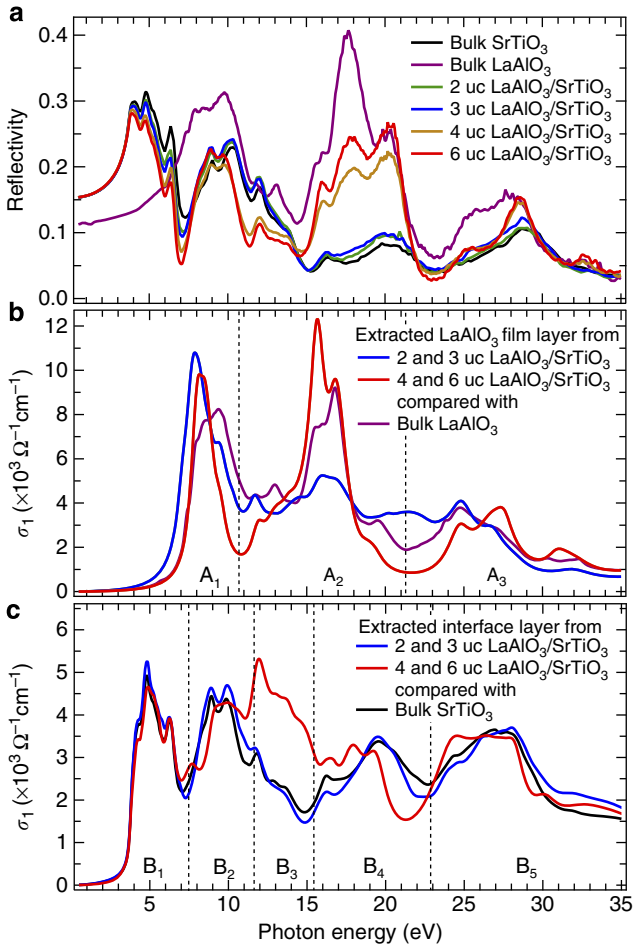

Figure 2 | Reflectivity and optical conductivity of each layer of $LaAlO_3$/$SrTiO_3$. (**a**) Reflectivity of $LaAlO_3/SrTiO_3$ as compared with bulk $LaAlO_3$ and bulk $SrTiO_3$. (**b**) Extracted optical conductivity (σ_1) of $LaAlO_3$ films at different thickness of $LaAlO_3$ film, compared with bulk $LaAlO_3$. (**c**) Extracted optical conductivity of the $LaAlO_3/SrTiO_3$ interface at different thickness of $LaAlO_3$ film, compared with bulk $SrTiO_3$. Note that the plots for 2 and 3 unit cells (uc) $LaAlO_3/SrTiO_3$ are the same because of the nature of the iteration analysis used to extract σ_1 from reflectivity, and the same is true for the 4 and 6 uc $LaAlO_3/SrTiO_3$. The σ_1 plots are divided into several energy regions, A_1–A_3 for $LaAlO_3$ and B_1–B_5 for $SrTiO_3$ and the interface. The regions are defined based on the distinct optical transitions associated with it, which in turn is based on theoretical calculations and previous reflectivity and valence electron energy loss spectroscopy[36–40].

to ~5 eV) spectroscopic ellipsometry is important. (Note that the spectroscopic ellipsometry data are crucial for the normalization of the derived dielectric functions from the reflectivity measurements made up to 35 eV as shown in Supplementary Methods.) The electronic band structures of the insulating and conducting $LaAlO_3/SrTiO_3$ are very different at high energy, and these differences are critical in revealing the true nature of $LaAlO_3/SrTiO_3$ interface. Furthermore, since reflectivity and spectroscopic ellipsometry are sensitive to unpercolated clusters of charges[31], the similarity of the reflectivity of insulating 2 and 3 uc $LaAlO_3/SrTiO_3$ also implies that there is no evidence of precursor of percolation effects in the insulating samples, especially the 3 uc $LaAlO_3/SrTiO_3$ (ref. 32).

Discussion

For detailed analysis, we turn our discussion to optical conductivity, σ_1, because it fulfils the optical f-sum rule, which is related to number of charges excited by the photons. For bulk materials like bulk $LaAlO_3$ and bulk $SrTiO_3$, σ_1 can be extracted directly from reflectivity using the Kramers–Kronig analysis[29,30]. On the other hand, $LaAlO_3/SrTiO_3$ is layered along the $<001>$ direction (perpendicular to the (001) surface of the sample) owing to its heterostructure nature as well as the presence of the conducting layer at $LaAlO_3/SrTiO_3$ interface. For this reason, the reflectivity of $LaAlO_3/SrTiO_3$ is analysed based on standard theory of wave propagation in a stratified media[33,34]. The analysis naturally leads to a three-layered structure for the conducting $LaAlO_3/SrTiO_3$: $LaAlO_3$ film layer on top, bulk $SrTiO_3$ substrate at the bottom and an interface layer sandwiched in between, representing the 2DEG of the conducting samples.

A self-consistent iteration procedure is used to extract the thickness and dielectric function of each layer, and as long as the iteration is convergent, the starting assumption of these parameters should have little effect, if any, on the final obtained values (see Supplementary Methods for details). From the analysis, it is found that the thickness of this interface layer is ~5 nm, consistent with previous observation using hard XPS[5], cross-sectional conducting tip AFM[35] and the upper limit for the superconducting layer thickness of $LaAlO_3/SrTiO_3$ (ref. 10). This result also suggests that the high-energy reflectivity can be used to measure the thickness of interface layer. For insulating $LaAlO_3/SrTiO_3$, the analysis naturally converges into an effective two-layered structure instead. This means for insulating $LaAlO_3/SrTiO_3$ the σ_1 at interface is very similar to that of bulk $SrTiO_3$ as discussed later. This can be easily understood owing to the absence of the conducting interface layer.

Now, σ_1 of each individual layer can be extracted separately, so that we can analyse the concomitant evolution of each individual layer of $LaAlO_3/SrTiO_3$ as the interface changes from insulating to conducting. Spectra of σ_1 for each layer are shown in Fig. 2b,c. It should be noted that the plots for 2 and 3 uc $LaAlO_3/SrTiO_3$ are the same owing to the nature of the iteration process (see Supplementary Methods), and the same is true for the 4 and 6 uc $LaAlO_3/SrTiO_3$.

For $LaAlO_3$, one can, based on band structure calculations[36,37], divide σ_1 into three main optical regions, while σ_1 of $SrTiO_3$ can be divided into five main optical regions[38–40]. Every transition is unique and originates from different orbitals in each layer and sublayer, and these are summarized in Table 1. Furthermore, the polarization of the incident light is also taken into account in assigning the optical transitions. Since the incident light is linearly polarized parallel to the sample surface, the majority of the optical transitions occur in the in-plane direction within each sublayer, allowing us to study spectral weight transfers between the different sublayers. For example, in A_1 region of $LaAlO_3$, the transition is from O_{La}-2*p* to La-4*d*, 5*f*, both of which reside within the LaO sublayer of $LaAlO_3$. The other transitions also follow this convention.

Figure 2b shows that σ_1 of $LaAlO_3$ film of insulating and conducting $LaAlO_3/SrTiO_3$ is dramatically different as compared with bulk $LaAlO_3$. Particularly, σ_1 in A_1 region of $LaAlO_3$ film in the insulating samples is higher than the bulk value, while for the conducting samples it is lower. Meanwhile, the reverse is true in A_2 region. It is very clear that there are spectral weight transfers occurring between these three regions when the thickness of $LaAlO_3$ film increases and the interface goes from insulating to conducting state.

It can be seen (Fig. 2c) that σ_1 of the interface layer to a significant extent resembles σ_1 of the bulk $SrTiO_3$. This indicates that the electronic interface layer is $SrTiO_3$-like, and that the conducting layer mostly resides in $SrTiO_3$ side rather than $LaAlO_3$. The most significant change in σ_1 happens at B_3 region when the interface becomes conducting. In bulk $SrTiO_3$, that

Table 1 | Main optical transitions of bulk $LaAlO_3$ and bulk $SrTiO_3$.

Region	Main optical transition	Photon energy (eV)
$LaAlO_3$		
A_1	O_{La}-2*p* → La-4*f*, 5*d*	0.5–10.6
A_2	O_{Al}-2*p* → Al-3*s*	10.6–21.5
A_3	O_{La}-2*s* → La-4*f*, 5*d* & O_{Al}-2*s* → Al-3*p*	21.5–35.0
$SrTiO_3$		
B_1	O_{Ti}-2*p* → Ti-3*d*-t_{2g}	0.5–7.1
B_2	O_{Ti}-2*p* → Ti-3*d*-e_g & O_{Sr}-2*p* → Sr-4*d*	7.1–11.3
B_3 (Only occurs at conducting interface)	Interface state → higher O_{Ti} orbitals	11.3–15.1
B_4	Sr-4*p* → Ti-3*d*	15.1–22.7
B_5	O_{Ti}-2*s* → Ti-3*d* & O_{Sr} → Sr-4*d*	22.7–35.0

The assignments are based on theoretical calculations and previous reflectivity and valence electron energy loss spectroscopy[36–40]. Note that the transition B_3 does not exist in bulk $SrTiO_3$ rather it is a new transition that arises from the new interface state at the conducting interface of $LaAlO_3/SrTiO_3$ as a characteristic of the two-dimensional electron gas (2DEG), which includes the newly occupied Ti-3*d*-t_{2g} states.

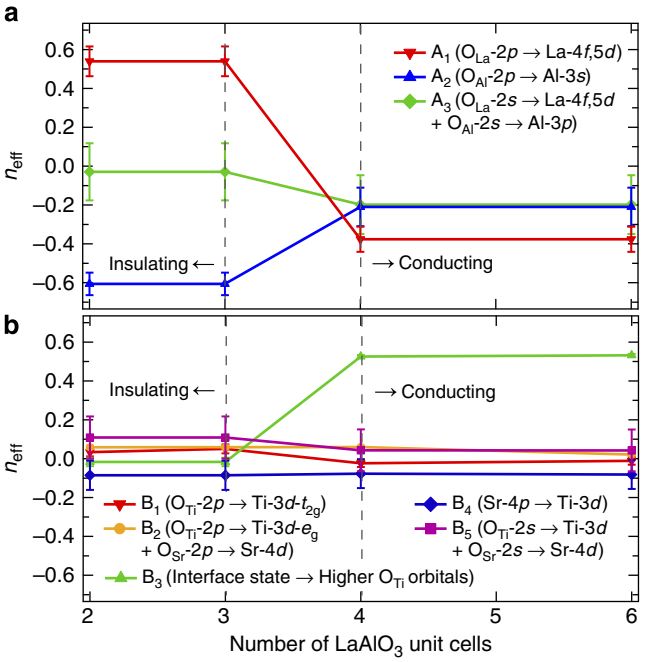

Figure 3 | The amount of charge redistribution and transfer in insulating and conducting $LaAlO_3/SrTiO_3$. (**a**) The amount of charge redistribution and transfer corresponding to different energy regions in the σ_1 plots of the $LaAlO_3$ film layer, relative to bulk $LaAlO_3$ values and plotted against $LaAlO_3$ film thickness. (**b**) The amount of charge redistribution and transfer corresponding to different energy regions in the σ_1 plots of the $LaAlO_3/SrTiO_3$ interface layer, relative to bulk $SrTiO_3$ values and plotted against $LaAlO_3$ film thickness. Each of these energy regions can be attributed to distinct optical transitions[36–40]. The error bars are obtained from the resolution limitation of the optics measurements and the errors introduced during the reflectivity normalization procedure.

region corresponds to a valley with no main optical transition. Interestingly, for the conducting samples a completely new peak emerges in that region. This implies that when the interface becomes conducting, a new characteristic interface state emerges representing the presence of the 2DEG. According to previous reports[3–7,17,19,22], the 2DEG resides in the Ti-3*d*-t_{2g} state of $SrTiO_3$, so this new interface state should also have Ti-3*d*-t_{2g} characteristic. Thus, based on the optical selection rules, the optical transition at B_3 region may be assigned to originate from this new interface state to unoccupied states of higher O orbitals (see Table 1). One should note that the σ_1 spectra of the interface layer of conducting $LaAlO_3/SrTiO_3$ does not show Drude response, consistent with previous infrared spectroscopic ellipsometry experiment[41].

The σ_1 analysis is very important because it can be linked to the effective number of electrons associated with a particular optical transition, N, using partial f-sum rule,

$$\frac{N}{V} = \frac{4m}{he^2}\int_{E_1}^{E_2} \sigma_1(E)dE, \qquad (1)$$

where e is the elementary charge, m is the electron mass and V is the unit volume. The E_1 and E_2 indicate the energy boundaries of that particular transition in the σ_1 plot. We then define n_{eff} as the N of each layer relative to either bulk $LaAlO_3$ (for $LaAlO_3$ film) or bulk $SrTiO_3$ (for interface layer) values. The advantage of this definition is that any changes in N in $LaAlO_3$ film or the interface layer can be distinguished from the bulk properties.

In $LaAlO_3/SrTiO_3$ (and thin films in general), the thickness of the $LaAlO_3$ film and interface layer is finite, so n_{eff} distributes over this finite thickness. If we assume that the distribution is uniform over each uc, the n_{eff} per uc, n_{uc}, can be defined such that

$$n_{eff} = \int_0^d n_{uc}dx = n_{uc}d, \qquad (2)$$

where d is the thickness in uc. In this case, the unit volume V becomes the volume occupied by each sublayer (LaO and AlO_2 for $LaAlO_3$ and SrO and TiO_2 for $SrTiO_3$), so that the unit of n_{uc} is the number of charge per sublayer. Thus, n_{eff}, which is the total amount of charge redistribution and transfer corresponding to a particular optical transition, can be obtained by integrating n_{uc} over the layer thickness, as shown in Fig. 3. (The procedure to obtain n_{eff} is further explained in Methods).

We start our discussion with insulating samples. As shown in Fig. 3a, n_{eff} of A_1 region of $LaAlO_3$ film increases by $\sim 0.5e^-$, while for A_2 region it decreases, also by $\sim 0.5e^-$. The net amount of the charge transfer in $LaAlO_3$ film is thus $(+0.5e^-) + (-0.5e^-) = 0$. This indicates a redistribution of $\sim 0.5e^-$ from O_{Al}-2*p* (AlO_2 sublayer) to O_{La}-2*p* (LaO sublayer), as shown in Table 1. On the basis of f-sum rule, this directly implies that there is no net charge transfer into the $LaAlO_3/SrTiO_3$ interface. As a result, the $LaAlO_3/SrTiO_3$ interface remains insulating. Since the $LaAlO_3$ film (and the system as a whole) remains insulating, the $\sim 0.5e^-$ charge redistribution does not result in the creation of electrons and holes in the LaO and AlO_2 sublayers but rather an increase of covalence between the LaO and AlO_2 sublayers, leading to the measured charge redistribution.

One way to interpret these data is by considering that the charge redistribution is uniform for all $LaAlO_3$ layers. In this case, the covalence of AlO_2 becomes modified from -1 to $-(1-n_{uc})$ and the covalence of LaO from $+1$ to $+(1-n_{uc})$ (Fig. 4a). The n_{uc} is $\sim 0.25e^- - 0.3e^-$ for the 2 uc $LaAlO_3/SrTiO_3$, and $\sim 0.17e^- - 0.2e^-$ for the 3 uc $LaAlO_3/SrTiO_3$ (see Methods). This charge redistribution within the $LaAlO_3$ sublayers (electronic reconstruction[2]) can thus help to decrease the potential build-up in the $LaAlO_3$ film and partially compensate the polarization catastrophe. Combined with ionic reconstruction mechanisms such as the buckling and ionic relaxations effects predicted[22,23]

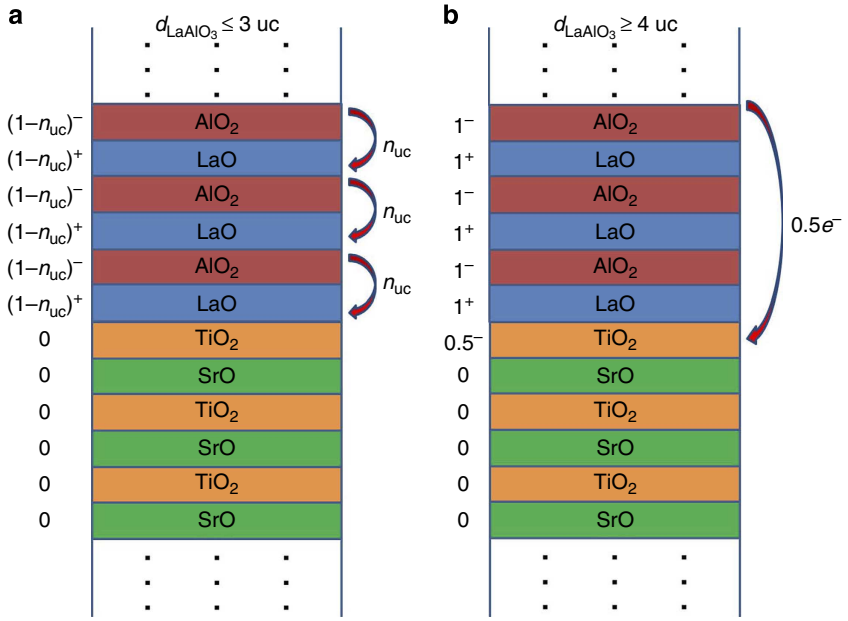

Figure 4 | Simplified pictorial layer-resolved electronic configuration model of $LaAlO_3/SrTiO_3$. (**a**) Layer-resolved electronic configuration model of insulating $LaAlO_3/SrTiO_3$, showing the charge redistribution from AlO_2 sublayer into LaO sublayer if the redistribution is assumed to be uniform across the $LaAlO_3$ film. The n_{uc} is $\sim 0.25e^- - 0.3e^-$ for the 2 uc $LaAlO_3/SrTiO_3$ and $\sim 0.17e^- - 0.2e^-$ for the 3 uc $LaAlO_3/SrTiO_3$. The charge redistribution can partially counteract the potential build-up due to polarization catastrophe[15,16] and keep the system insulating. (**b**) Layer-resolved electronic configuration model of conducting $LaAlO_3/SrTiO_3$, showing the overall charge transfer of $0.5e^-$ from $LaAlO_3$ film into the $LaAlO_3/SrTiO_3$ interface, consistent with the polarization catastrophe model. In this simple picture, the extra $0.5e^-$ is depicted to reside only within the first uc of interface, while in our results it is distributed over the ~ 5 nm thickness on the interface. To ensure charge conservation, one of the upper layers of $LaAlO_3$ (that is, in the dot-signed region above the depicted third layer of $LaAlO_3$) should have AlO_2 sublayer with valence state of $(AlO_2)^{0.5-}$ instead of $(AlO_2)^-$.

and observed earlier using surface X-ray diffraction[24,25] and second harmonic generation[32], what we are measuring in terms of charge redistribution may arise from such a mechanism.

Another possible scenario that can be considered to interpret the data is that, instead of involving the whole $LaAlO_3$ layers, the charge redistribution only happens at the topmost (that is, surface) $LaAlO_3$ layer. In this case, the covalence of surface AlO_2 becomes modified from -1 to -0.5 and the covalence of surface LaO from $+1$ to $+0.5$, but the deeper $LaAlO_3$ layer remains unchanged, since the charge redistribution is confined only in the surface (that is, surface reconstruction). In this scenario, the surface charge redistribution is still able to partially compensate the polarization catastrophe, but it is in less of an agreement with the buckling effects, since the buckling was observed experimentally, and supported by theoretical calculations[22–25], to affect the whole $LaAlO_3$ film, and not only the surface.

On the other hand, for conducting samples we observe a different phenomenon. The n_{eff} of both A_1 and A_2 regions of $LaAlO_3$ film decreases (Fig. 3a). For A_1 region it decreases by $\sim 0.3e^- - 0.4e^-$, while for A_2 region it decreases by $\sim 0.2e^-$, leading to an overall $\sim 0.5e^-$ decrease of n_{eff} in the $LaAlO_3$ film. At the same time, for the interface layer the most significant change that happens when $LaAlO_3/SrTiO_3$ becomes conducting is the increase of n_{eff} of B_3 region by $\sim 0.5e^-$ (Fig. 3b). The total charge transfer within the whole $LaAlO_3/SrTiO_3$ sample is thus again 0, with the decrease of $\sim 0.5e^-$ in $LaAlO_3$ film compensated by the increase of $\sim 0.5e^-$ at the interface. On the basis of f-sum rule, this clearly indicates that there is a charge transfer of $\sim 0.5e^-$ from the $LaAlO_3$ film into the interface to form the 2DEG (Fig. 4b), consistent with the polarization catastrophe model[15,16]. On the basis of the definition of n_{eff}, this $\sim 0.5e^-$ extra charge at the interface is distributed over the ~ 5 nm thickness of the interface (which mostly resides in the $SrTiO_3$ side).

Moreover, it can be seen from Fig. 2c that the B_3 peak, which involves the transition from the new interface state that contains this $\sim 0.5e^-$ extra charge, is very broad (~ 4 eV wide), which means that the $\sim 0.5e^-$ is distributed over a rather wide energy range. This may be one of the reasons why transport experiments can only measure a fraction of this $\sim 0.5e^-$, since only a small portion of the charge is delocalized and thus able to contribute to electrical conductivity.

Furthermore, Fig. 3b also shows that the n_{eff} of B_1 and B_5 regions, both of which involve transitions into the unoccupied Ti-3d-t_{2g} states, decrease by $\sim 0.05e^-$ (that is, $\sim 10\%$ of $0.5e^-$). This implies that the new interface state of conducting $LaAlO_3/SrTiO_3$ has Ti-3d-t_{2g} characteristic[3–7,17,19,22], so the extra $\sim 0.5e^-$ also partially fills the previously unoccupied Ti-3d-t_{2g} state of $SrTiO_3$. This decrease is consistent with previous observations using X-ray absorption spectroscopy experiments[3,6]. In X-ray absorption spectroscopy at Ti-$L_{3,2}$ edges of conducting $LaAlO_3/SrTiO_3$, the excitation to the unoccupied Ti-3d-t_{2g} states also decreases compared with bulk $SrTiO_3$. Intriguingly, these decreases are much smaller if one assumes that all of the $\sim 0.5e^-$ extra charge partially fills the Ti-3d-t_{2g}-unoccupied density of state (DOS). This is because, based on this assumption, one would expect to observe the decrease of Ti-3d-t_{2g}-unoccupied DOS (and thus the n_{eff} of B_1 and B_5 regions) in conducting $LaAlO_3/SrTiO_3$ also by an equivalent of $\sim 0.5e^-$. However, this is not the case, which implies that the $\sim 0.5e^-$ extra charge contained within the new interface state does not only reduce the number of unoccupied Ti-3d DOS, but surprisingly also other states at even higher energies, implying the importance of strong correlations and hybridizations effects in explaining the interlayer charge transfer in conducting $LaAlO_3/SrTiO_3$ (refs 26,42,43).

Another interesting observation to note is that in the conducting samples, the n_{eff} of A_3 region of $LaAlO_3$ film also

decreases by $\sim 0.2e^-$. The transition in this region corresponds to O-2*s* state, which is strongly localized and directly corresponds to the availability of oxygen in the $LaAlO_3$ film. Thus, the decrease of O-2*s* DOS can indicate the presence of oxygen vacancies in the $LaAlO_3$ film of the conducting samples. For 4 uc $LaAlO_3/SrTiO_3$, there are $24e^-$ in O-2*s* state of $LaAlO_3$; thus, the $\sim 0.2e^-$ decrease is equivalent to $\sim 1\%$ oxygen vacancy. This is interesting because it has been suggested that the presence of oxygen vacancies in $LaAlO_3$ film may enhance the charge transfer from $LaAlO_3$ film into $LaAlO_3/SrTiO_3$ interface[7,44,45]. Because of the charge transfer into the interface, the $LaAlO_3$ film lacks $\sim 0.5e^-$ (that is, has additional ~ 0.5 holes), so the extra e^- created by the oxygen vacancy may partially compensate these holes and stabilize the charge transfer. Interestingly, in insulating $LaAlO_3/SrTiO_3$, this oxygen vacancies signature is not observed.

It is noteworthy to reconcile our results with photoconductivity effects observed in $LaAlO_3/SrTiO_3$. Previous transport results[46,47] have shown that when $LaAlO_3/SrTiO_3$ was illuminated by photons with energies higher than the $SrTiO_3$ bandgap, its conductivity could increase because of the presence of photo-generated carriers. On the basis of hard XPS data[5], the amount of these photo-generated carriers is estimated to be 2.1×10^{13} cm^{-2} ($\sim 0.03e^-$), which is much smaller than the number of e^- contributed to the charge transfer and charge redistributions observed in our results ($\sim 0.5e^-$). Thus, the photoconductivity effects might only influence the estimated n_{eff} by $\sim 6\%$, and do not affect our analysis adversely.

Recent observations have also indicated that the cationic stoichiometry, for example, the La/Al ratio in $LaAlO_3$ film, may affect the electrical properties of $LaAlO_3/SrTiO_3$ (refs 18,48,49). How this cationic stoichiometric effects would influence the high-energy optical conductivity of insulating and conducting $LaAlO_3/SrTiO_3$ is an important open question. Thus, its interplay with the charge transfer and redistribution phenomena as observed in high-energy optical conductivity still remains to be answered.

In summary, we have shown that high-energy reflectivity and spectroscopic ellipsometry studies of $LaAlO_3/SrTiO_3$ have revealed significant differences between the charge redistribution of insulating (2 and 3 uc of $LaAlO_3$) and charge transfer mechanisms of conducting (4 and 6 uc of $LaAlO_3$) $LaAlO_3/SrTiO_3$. In insulating $LaAlO_3/SrTiO_3$, $\sim 0.5e^-$ charge redistribution is observed between the AlO_2 and LaO sublayers and partially compensates the polarization catastrophe. In the conducting samples, $\sim 0.5e^-$ is measured to be transferred from $LaAlO_3$ film into the interface, which is consistent with the polarization catastrophe model. We believe that this study reveals the nature of the intra- and interlayer charge redistributions and charge transfers in $LaAlO_3/SrTiO_3$, and hence opens a path to understand the various electronic reconstructions involving the interfaces of complex oxides heterostructures. Furthermore, the use of high-energy reflectivity coupled with spectroscopic ellipsometry could be extended to other similar polar and nonpolar oxide interface systems.

Methods

Sample preparation. $LaAlO_3/SrTiO_3$ samples were prepared by growing $LaAlO_3$ film on top of (001) $SrTiO_3$ substrates obtained from Crystec using pulsed laser deposition[12]. Before the growth, the $SrTiO_3$ substrates were treated using HF and are annealed at 950 °C for 2 h in O_2 flow to achieve the desired TiO_2 surface termination[50]. The AFM topography image of the TiO_2-terminated $SrTiO_3$ substrate in Fig. 1a clearly shows the atomically flat surface with uc steps. The growth target was $LaAlO_3$ single crystal, also obtained from Crystec. The deposition pressure was 10^{-3} Torr, with background pressure of 10^{-9} Torr. The deposition temperature was 750 °C, with cooling rate of 10 °C min^{-1} at the deposition pressure. The laser pulse frequency was 1 Hz. Four samples with varying thickness of 2, 3, 4 and 6 uc of $LaAlO_3$ film were made, as monitored using reflective high-energy electron diffraction (Fig. 1b). After $LaAlO_3$ deposition, AFM topography measurements show that the atomically flat surface with uc step and terrace structure of $SrTiO_3$ is preserved, with surface roughness of ~ 1 Å (see Fig. 1c,d).

Optics measurements. The optical conductivity were obtained using a combination of spectroscopic ellipsometry (0.5–5.6 eV) and UV–VUV reflectivity (3.7–35 eV) measurements[26–28]. The details of the optical measurements are as follow. The spectroscopic ellipsometry measurements were performed in the spectral range between 0.5 and 5.6 eV by using an SE 850 ellipsometer at room temperature[51]. Three different incident angles of 60°, 70° and 80° from the sample normal were used, and the incident light was 45° linearly polarized from the plane of incident. For reflectivity measurements in the high-energy range between 3.7 and 35 eV, we used the SUPERLUMI beamline at the DORIS storage ring of HASYLAB (DESY)[52]. The incoming photon was incident at the angle of 17.5° from the sample normal with linear polarization parallel to the sample surface. The sample chamber was outfitted with a gold mesh to measure the incident photon flux after the slit of the monochromator. The measurements were performed in ultrahigh vacuum environment (chamber pressure of 5×10^{-10} mbar) at room temperature. before these measurements, the samples were heated up to 400 K in ultrahigh vacuum to ensure that there was no additional adsorbate layers on the surface of the samples. The obtained UV–VUV reflectivity data were calibrated by comparing it with the

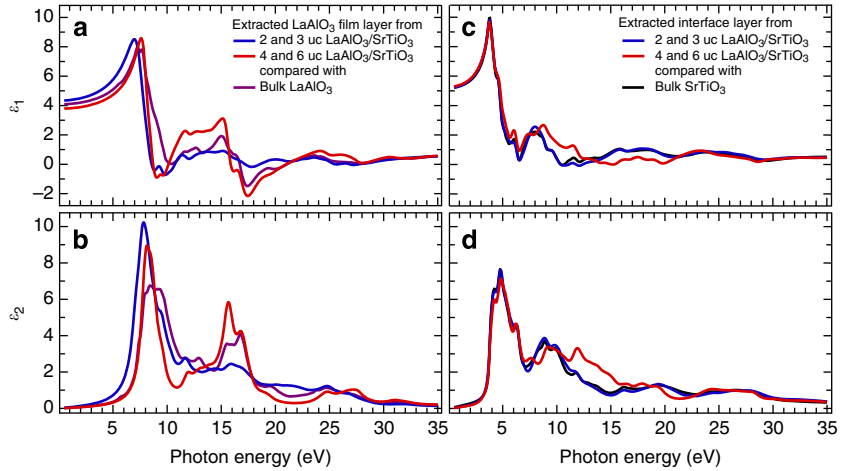

Figure 5 | Complex dielectric function of each layer of $LaAlO_3/SrTiO_3$. (**a**) Real part of complex dielectric function (ε_1) of $LaAlO_3$ film, compared with bulk $LaAlO_3$. (**b**) Imaginary part of complex dielectric function (ε_2) of $LaAlO_3$ film, compared with bulk $LaAlO_3$. (**c**) The ε_1 of $LaAlO_3/SrTiO_3$ interface, compared with bulk $SrTiO_3$. (**d**) The ε_2 of $LaAlO_3/SrTiO_3$ interface, compared with bulk $SrTiO_3$. Note that the plots for 2 and 3 unit cells (uc) are the same because of the nature of the thickness-dependent iteration, and the same is true for the 4 and 6 uc case.

luminescence yield of sodium salicylate ($NaC_7H_5O_3$) and the gold mesh current. These as-measured UV–VUV reflectivity data were further normalized by using the self-normalized reflectivity extracted from spectroscopic ellipsometry[34,51], and the two normalized data were appended to obtain the combined reflectivity from 0.5 to 35 eV (see Supplementary Fig. 1).

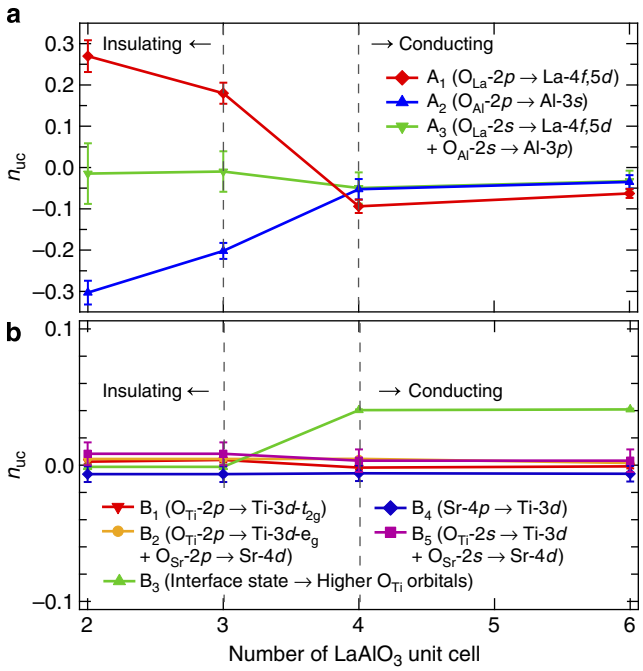

Figure 6 | Effective number of charge per unit cell (uc) of $LaAlO_3$ and interface layer of $LaAlO_3/SrTiO_3$. (**a**) The effective number of charge per uc, n_{uc}, of $LaAlO_3$ film, if the charge distribution is assumed to be uniform over the $LaAlO_3$ thicknesses (2, 3, 4 and 6 uc). (**b**) The n_{uc} of the $LaAlO_3$/$SrTiO_3$ interface, if the charge distribution is assumed to be uniform over the interface thickness (~5.3 nm). Each of these energy regions can be attributed to distinct optical transitions[36–40]. The error bars are obtained from the resolution limitation of the optics measurements and the errors introduced during the reflectivity normalization procedure.

Analysis of optics data. Both the spectroscopic ellipsometry and the combined reflectivity data were analysed using a combination of the Drude–Lorentz oscillator multilayer fitting[33,34] and self-consistent iteration method (see Supplementary Methods). Owing to its multilayered nature, the $LaAlO_3/SrTiO_3$ samples, especially the conducting cases, are considered to have the following three layers: the $LaAlO_3$ film on top, the $SrTiO_3$ substrate at the bottom and the interface layer in between (see Supplementary Fig. 2), consistent with previous observation using cross-sectional conducting tip AFM[35]. Since the spectroscopic ellipsometry data were taken at three different incident angles of 60°, 70° and 80°, it was fitted using angle-dependent iteration method (see Supplementary Methods), and the fitting results are shown in Supplementary Figs 3, 4, 5, 6 and 7. Supplementary Figure 4 also shows that the thickness of the conducting interface layer is ~5 nm, consistent with previous observations[5,10,35]. Furthermore, from these variable angle spectroscopic ellipsometry results, the absence of absorbate layer and the absence of significant anisotropy can also be inferred. On the other hand, the normalized UV–VUV reflectivity data were fitted using thickness-dependent iteration method (see Supplementary Methods), and the results of the fitting are shown in Supplementary Fig. 8.

Complex dielectric function of $LaAlO_3/SrTiO_3$. From the analysis described above, the complex dielectric function, $\varepsilon(\omega)$, of each layer of $LaAlO_3/SrTiO_3$ can be extracted from the high-energy reflectivity of $LaAlO_3/SrTiO_3$ (Fig. 2a), as presented in Fig. 5. In turn, this $\varepsilon(\omega)$ can be converted into optical conductivity σ_1 using $\sigma_1(\omega) = \varepsilon_0\varepsilon_2(\omega)\omega$, as presented in Fig. 2b,c. In Fig. 5a,b, it can be seen that the $\varepsilon(\omega)$ of the $LaAlO_3$ film layer for both insulating and conducting $LaAlO_3/SrTiO_3$ is very different than that of bulk $LaAlO_3$, which shows that the band structure of $LaAlO_3$ film is very different than bulk $LaAlO_3$. Meanwhile, the $\varepsilon(\omega)$ at the interface of the insulating samples (2 and 3 uc $LaAlO_3/SrTiO_3$, see Fig. 5c) is very similar to that of bulk $SrTiO_3$, which can be explained by the absence of the 2DEG in the insulating samples. Interestingly, for the conducting samples (4 and 6 uc $LaAlO_3/SrTiO_3$, see Fig. 5d) there are new features around 8–12 eV for ε_1 and 11–16 eV for ε_2, which, on further analysis (see Discussions), are related to the presence of the conducting interface in those sample.

Estimation of charge transfer and redistribution. From equations (1) and (2), we can extract the n_{uc}, which is the amount of charge redistribution and transfer per uc associated with a particular optical transition relative to the bulk values. To get the accurate number, we need to carefully consider within what volume V in the uc the electrons reside. Both $LaAlO_3$ and $SrTiO_3$ crystal structures can be thought of as an alternating layer structure. $LaAlO_3$ consists of alternating polar $(LaO)^+$ and $(AlO_2)^-$ sublayers, while $SrTiO_3$ consists of alternating nonpolar SrO and TiO_2 sublayers (see Figs 1d and 4). Owing to this layered structure, in a first approximation each cation (La and Al for $LaAlO_3$, Sr and Ti for $SrTiO_3$) only occupies a volume of half uc (instead of the full one uc). For example, the La of $LaAlO_3$ has to share the space of one uc with Al (with each getting half), and similarly the Sr of $SrTiO_3$ has to share with Ti. Furthermore, for $LaAlO_3$, the valence electrons of the O atoms that belong to the two different sublayers (LaO and AlO_2) contribute to two different optical transitions in the σ_1 spectra (Fig. 2b

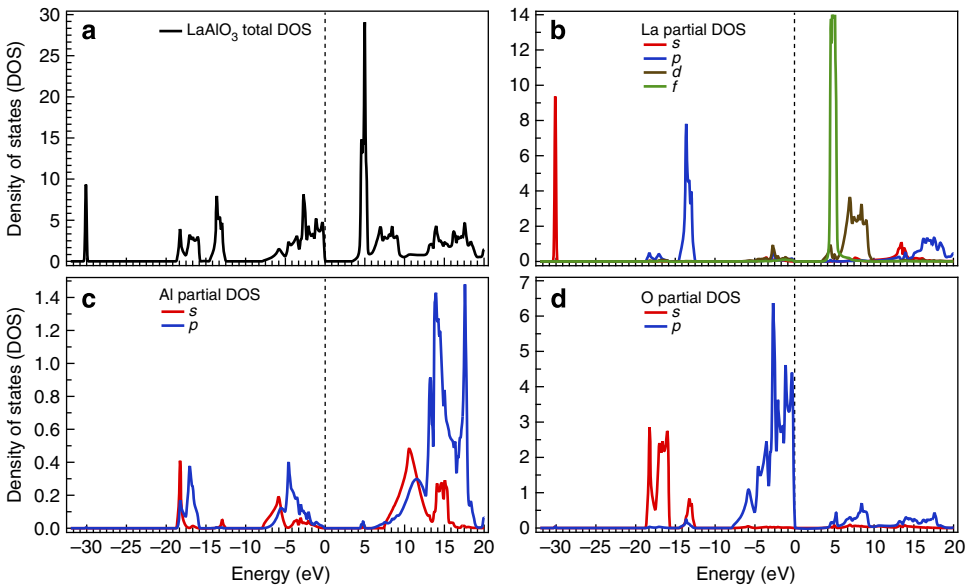

Figure 7 | Theoretical band structure of $LaAlO_3$. (**a**) Total density of states (DOS) of $LaAlO_3$. (**b**) Partial DOS of La. (**c**) Partial DOS Al. (**d**) Partial DOS of O. The dotted lines are the Fermi level.

and Table 1). For simplicity, O_{La} is defined as the O in the LaO plane and O_{Al} as the O in the AlO_2 plane. Thus, O_{La} also has to share the space of one uc with O_{Al}, with each getting the space of half uc. The same is true for $SrTiO_3$, where the O_{Sr} in the SrO plane also has to share the space of one uc with the O_{Ti} in the TiO_2 plane. This implies that the valence electrons belonging to the different ions can also be approximated to reside in a volume of half uc. For this reason, to obtain the n_{uc} the volume V is chosen to be the volume of half uc of $LaAlO_3$ (lattice constant $a_0 = 3.81$ Å) or $SrTiO_3$ ($a_0 = 3.905$ Å), whichever applicable. This consideration makes the unit of n_{uc} to be the number of charge per sublayer. The result for this n_{uc} estimation is shown in Fig. 6. For 2 uc $LaAlO_3/SrTiO_3$, the n_{uc} is $\sim 0.25e^- - 0.3e^-$, while for 3 uc $LaAlO_3/SrTiO_3$, the n_{uc} is $\sim 0.17e^- - 0.2e^-$. Then, the n_{eff}, which is the total amount of charge redistribution and transfer corresponding to a particular optical transition can be obtained by integrating n_{uc} over the layer thickness, as shown in Fig. 3.

The error bars in Figs 3 and 6 are estimated as follows. It is assumed that there are two main sources of random errors in the data: from the resolution limitation of the optics measurements (estimated to be $\sim 2\%$) and from the errors introduced in the normalization process (estimated to be $\sim 5\%$). These errors affect the reflectivity data (that is, ΔR), and to obtain the corresponding errors for σ_1 ($\Delta\sigma$) and thus n_{eff}, the errors are propagated using

$$\left|\frac{\Delta\sigma}{\sigma}\right| = \left|\frac{\Delta\varepsilon}{\varepsilon}\right| = \left|1 - \frac{1}{\sqrt{\varepsilon}} - \frac{1}{\varepsilon}\right|\left|\frac{\Delta R}{R}\right|. \quad (3)$$

$LaAlO_3$ band structure calculation. Unlike $SrTiO_3$ that has been studied very thoroughly[38–40], previous reports that study the band structure and high photon-energy properties of $LaAlO_3$ in a detailed and comprehensive manner remain quite scarce[36,37]. Because of this, we performed our own band structure calculation of $LaAlO_3$ to complement those previous studies. The results can be used as a tool to determine the high photon-energy optical transition assignments of $LaAlO_3$, as listed in Table 1.

The details of the calculation are as follows. Cubic $LaAlO_3$ has a space group of Pm3m with an experimental lattice parameters of $a = b = c = 3.8106$ Å at 821 K (ref. 53). The calculations were performed using CASTEP code[54]. Geometry optimization had been carried out with local density approximation functional using cutoff energy of 1,500 eV and a $15 \times 15 \times 15$ Monkhorst–Pack grid[55] that corresponds to 120 **k**-points in the irreducible Brillouin zone. The cutoff energy and **k**-point mesh had been tested and converged to energy differences of 1×10^{-5} and 4×10^{-5} eV per atom, respectively. Ultrasoft pseudopotentials were generated 'on the fly' with valence states 4*f*, 5*s*, 5*p*, 5*d*, 6*s* for La, 3*s*, 3*p* for Al and 2*s*, 2*p* for O. The electronic minimization method used for the self-consistent field calculation was density mixing[56] with a self-consistent field tolerance of 2.0×10^{-6} eV per atom. The geometry optimization was carried out by the Broyden–Fletcher–Goldfarb–Shanno algorithm[57] with energy, force and displacement tolerances of 5.0×10^{-6} eV per atom, 1.0×10^{-2} eV Å^{-1} and 5.0×10^{-4} Å, respectively. The optimized lattice parameter was found out to be 3.73 Å. Converged DOS calculation was carried out with a **k**-mesh of $20 \times 20 \times 20$ and consistent with previous calculations[36,37]. The calculation results are displayed in Fig. 7.

References

1. Hwang, H. Y. *et al.* Emergent phenomena at oxide interfaces. *Nat. Mater.* **11,** 103–113 (2012).
2. Hesper, R., Tjeng, L. H., Heeres, A. & Sawatzky, G. A. Photoemission evidence of electronic stabilization of polar surfaces in K_3C_{60}. *Phys. Rev. B* **62,** 16046–16055 (2000).
3. Siemons, W. *et al.* Origin of charge density at $LaAlO_3$ on $SrTiO_3$ heterointerfaces: Possibility of intrinsic doping. *Phys. Rev. Lett.* **98,** 196802 (2007).
4. Salluzzo, M. *et al.* Orbital reconstruction and the two-dimensional electron gas at the $LaAlO_3/SrTiO_3$ interface. *Phys. Rev. Lett.* **102,** 166804 (2009).
5. Sing, M. *et al.* Profiling the interface electron gas of $LaAlO_3/SrTiO_3$ heterostructures with hard X-ray photoelectron spectroscopy. *Phys. Rev. Lett.* **102,** 176805 (2009).
6. Berner, G. *et al.* $LaAlO_3/SrTiO_3$ oxide heterostructures studied by resonant inelastic X-ray scattering. *Phys. Rev. B* **82,** 241405(R) (2010).
7. Berner, G. *et al.* Direct k-space mapping of the electronic structure in an oxide-oxide interface. *Phys. Rev. Lett.* **110,** 247601 (2013).
8. Ohtomo, A. & Hwang, H. Y. A high-mobility electron gas at the $LaAlO_3/SrTiO_3$ heterointerface. *Nature* **427,** 423–426 (2004).
9. Thiel, S., Hammerl, G., Schmehl, A., Schneider, C. W. & Mannhart, J. Tunable quasi–two-dimensional electron gases in oxide heterostructures. *Science* **313,** 1942–1945 (2006).
10. Reyren, N. *et al.* Superconducting interfaces between insulating oxides. *Science* **317,** 1196–1199 (2007).
11. Brinkman, A. *et al.* Magnetic effects at the interface between non-magnetic oxides. *Nat. Mater.* **6,** 493–496 (2007).
12. Ariando *et al.* Electronic phase separation at the $LaAlO_3/SrTiO_3$ interface. *Nat. Commun.* **2,** 188–194 (2011).
13. Li, L., Richter, C., Mannhart, J. & Ashoori, R. C. Coexistence of magnetic order and two-dimensional superconductivity at $LaAlO_3/SrTiO_3$ interfaces. *Nat. Phys.* **7,** 762–766 (2011).
14. Bert, J. A. *et al.* Direct imaging of the coexistence of ferromagnetism and superconductivity at the $LaAlO_3/SrTiO_3$ interface. *Nat. Phys.* **7,** 767–771 (2011).
15. Harrison, W. A., Kraut, E. A., Waldrop, J. R. & Grant, R. W. Polar heterojunction interfaces. *Phys. Rev. B* **18,** 4402–4410 (1978).
16. Nakagawa, N., Hwang, H. Y. & Muller, D. A. Why some interfaces cannot be sharp. *Nat. Mater.* **5,** 204–209 (2006).
17. Popović, Z. S., Satpathy, S. & Martin, R. M. Origin of the two-dimensional electron gas carrier density at the $LaAlO_3$ on $SrTiO_3$ interface. *Phys. Rev. Lett.* **101,** 256801 (2008).
18. Warusawithana, M. P. *et al.* $LaAlO_3$ stoichiometry is key to electron liquid formation at $LaAlO_3/SrTiO_3$ interfaces. *Nat. Commun.* **4,** 2351 (2013).
19. Lee, J. & Demkov, A. A. Charge origin and localization at the *n*-type $SrTiO_3/LaAlO_3$ interface. *Phys. Rev. B* **78,** 193104 (2008).
20. Segal, Y., Ngai, J. H., Reiner, J. W., Walker, F. J. & Ahn, C. H. X-ray photoemission studies of the metal-insulator transition in $LaAlO_3/SrTiO_3$ structures grown by molecular beam epitaxy. *Phys. Rev. B* **80,** 241107(R) (2009).
21. Takizawa, M., Tsuda, S., Susaki, T., Hwang, H. Y. & Fujimori, A. Electronic charges and electric potential at $LaAlO_3/SrTiO_3$ interfaces studied by core-level photoemission spectroscopy. *Phys. Rev. B* **84,** 245124 (2011).
22. Pentcheva, R. & Pickett, W. E. Avoiding the polarization catastrophe in $LaAlO_3$ overlayers on $SrTiO_3$ (001) through polar distortion. *Phys. Rev. Lett.* **102,** 107602 (2009).
23. Pentcheva, R. *et al.* Parallel electron-hole bilayer conductivity from electronic interface reconstruction. *Phys. Rev. Lett.* **104,** 166804 (2010).
24. Pauli, S. A. *et al.* Evolution of the interfacial structure of $LaAlO_3$ on $SrTiO_3$. *Phys. Rev. Lett.* **106,** 036101 (2011).
25. Saluzzo, M. *et al.* Structural and electronic reconstructions at the $LaAlO_3/SrTiO_3$ interface. *Adv. Mater.* **25,** 2333–2338 (2013).
26. Rusydi, A. *et al.* Metal-insulator transition in manganites: changes in optical conductivity up to 22 eV. *Phys. Rev. B* **78,** 125110 (2008).
27. Majidi, M. A., Su, H., Feng, Y. P., Rübhausen, M. & Rusydi, A. Theory of high-energy optical conductivity and the role of oxygens in manganites. *Phys. Rev. B* **84,** 075136 (2011).
28. Santoso, I. *et al.* Observation of room-temperature high-energy resonant excitonic effects in graphene. *Phys. Rev. B* **84,** 081403(R) (2011).
29. Jahoda, F. C. Fundamental absorption of barium oxide from its reflectivity spectrum. *Phys. Rev.* **107,** 1261–1265 (1957).
30. Nilsson, P. O. & Munkby, L. Investigation of errors in the Kramers-Kronig analysis of reflectance data. *Phys. Kondens. Mater.* **10,** 290–298 (1969).
31. Rauer, R. *et al.* Thickness dependent phase separation in $La_{0.7}Ca_{0.3}MnO_3$ films. *Appl. Phys. Lett.* **81,** 3777–3779 (2002).
32. Savoia, A. *et al.* Polar catastrophe and electronic reconstructions at the $LaAlO_3/SrTiO_3$ interface: evidence from optical second harmonic generation. *Phys. Rev. B* **80,** 075110 (2009).
33. Born, M. & Wolf, E. *Principles of Optics*. Chapter 1. Cambridge University Press, 2003).
34. Fujiwara, H. *Spectroscopic Ellipsometry: Principles and Applications* (Wiley, 2007).
35. Basletic, M. *et al.* Mapping the spatial distribution of charge carriers in $LaAlO_3/SrTiO_3$ heterostructures. *Nat. Mater.* **7,** 621–625 (2008).
36. Knizhnik, A. A. *et al.* First-principles calculations of the electrical properties of $LaAlO_3$ and its interface with Si. *Phys. Rev. B* **72,** 235329 (2005).
37. Luo, X. & Wang, B. First-principles study of the electronic and optical properties in rhombohedral $LaAlO_3$. *J. Appl. Phys.* **104,** 053503 (2008).
38. Cardona, M. Optical properties and band structure of $SrTiO_3$ and $BaTiO_3$. *Phys. Rev.* **140,** A651–A655 (1965).
39. Van Benthem, K., Elsässer, C. & French, R. H. Bulk electronic structure of $SrTiO_3$: experiment and theory. *J. Appl. Phys.* **90,** 6156–6164 (2001).
40. Sponza, L., Véniard, V., Sottile, F., Giorgetti, C. & Reining, L. Role of localized electrons in electron-hole interaction: The case of $SrTiO_3$. *Phys. Rev. B* **87,** 235102 (2013).
41. Dubroka, A. *et al.* Dynamical response and confinement of the electrons at the $LaAlO_3/SrTiO_3$ interface. *Phys. Rev. Lett.* **104,** 156807 (2010).
42. Eskes, H., Meinders, M. B. J. & Sawatzky, G. A. Anomalous transfer of spectral weight in doped strongly correlated systems. *Phys. Rev. Lett.* **67,** 1035–1038 (1991).
43. Meinders, M. B. J., Eskes, H. & Sawatzky, G. A. Spectral-weight transfer: breakdown of low-energy-scale sum rules in correlated systems. *Phys. Rev. B* **48,** 3916–3926 (1993).
44. Zhang, L. *et al.* Origin of insulating behavior of the p-type $LaAlO_3/SrTiO_3$ interface: polarization-induced asymmetric distribution of oxygen vacancies. *Phys. Rev. B* **82,** 125412 (2010).

45. Li, Y., Phattalung, S. N., Limpijumnong, S., Kim, J. & Yu, J. Formation of oxygen vacancies and charge carriers induced in the *n*-type interface of a $LaAlO_3$ overlayer on $SrTiO_3$(001). *Phys. Rev. B* **84,** 245307 (2011).
46. Huijben, M. *et al.* Electronically coupled complementary interfaces between perovskite band insulators. *Nat. Mater.* **5,** 556–560 (2006).
47. Tebano, A., Fabbri, E., Pergolesi, D., Balestrino, G. & Traversa, E. Room-temperature giant persistent photoconductivity in $SrTiO_3/LaAlO_3$ heterostructures. *ACS Nano* **6,** 1278–1283 (2012).
48. Dildar, I. M. *et al.* Non-conducting interfaces of $LaAlO_3/SrTiO_3$ produced in sputter deposition: the role of stoichiometry. *Appl. Phys. Lett.* **102,** 121601 (2013).
49. Breckenfeld, E. *et al.* Effect of growth induced (non)stoichiometry on interfacial conductance in $LaAlO_3/SrTiO_3$. *Phys. Rev. Lett.* **110,** 196804 (2013).
50. Koster, G., Kropman, B. L., Rijnders, G. J. H. M., Blank, D. H. A. & Rogalla, H. Quasi-ideal strontium titanate crystal surfaces through formation of strontium hydroxide. *Appl. Phys. Lett.* **73,** 2920–2922 (1998).
51. Rauer, R., Neuber, G., Kunze, J., Bäckström, J. & Rübhausen, M. Temperature-dependent spectral generalized magneto-optical ellipsometry for ferromagnetic compounds. *Rev. Sci. Instrum.* **76,** 023910 (2005).
52. Zimmerer, G. Status report on luminescence investigations with synchrotron radiation at HASYLAB. *Nucl. Instrum. Methods Phys. Res. A* **308,** 178–186 (1991).
53. Howard, C. J., Kennedy, B. J. & Chakoumakos, B. C. Neutron powder diffraction study of rhombohedral rare-earth aluminates and the rhombohedral to cubic phase transition. *J. Phys. Condens. Matter* **12,** 349–365 (2000).
54. Clark, S. J. *et al.* First principles methods using CASTEP. *Z. Kristallogr.* **220,** 567–570 (2005).
55. Monkhorst, H. J. & Pack, J. D. Special points for Brillouin-zone integrations. *Phys. Rev. B* **13,** 5188–5192 (1976).
56. Kresse, G. & Furthmuller, J. Efficient iterative schemes for ab initio total-energy calculations using a plane-wave basis set. *Phys. Rev. B* **54,** 11169–11186 (1996).
57. Pfrommer, B. G., Cote, M., Louie, S. G. & Cohen, M. L. Relaxation of crystals with the quasi-Newton method. *J. Comput. Phys.* **131,** 233–240 (1997).

Acknowledgements

We acknowledge George Sawatzky, Warren Picket, Anthony J Leggett, Michael Coey, Daniel Khomskii and Wei Ku for the discussions and their valuable comments. This work is supported by Singapore National Research Foundation under its Competitive Research Funding (NRF-CRP 8-2011-06 and NRF2008NRF-CRP002024), MOE-AcRF Tier-2 (MOE2010-T2-2-121), NUS-YIA, FRC, BMBF under 50KS7GUD as well as DFG through Ru 773/5-1. We acknowledge the CSE-NUS computing centre for providing facilities for our numerical calculations.

Author contributions

A.R. designed the high-energy optical reflectivity coupled with spectroscopy ellipsometry experiments to study electronic reconstruction at buried interfaces. T.C.A., I.S., P.K.G., A.K. and A.R. performed high-energy optical reflectivity and spectroscopy ellipsometry measurements. A.A., A. and T.V. grew high-quality thin films and performed X-ray diffraction, AFM topography and transport measurements. H.M.O. and A.R. provided the band structure calculations. T.C.A. and A.R. carried out detail data analysis and discussed the results with all co-authors. T.C.A. and A.R. wrote the paper with inputs from all co-authors. A.R. planned and supervised the project.

Additional information

Supplementary Information accompanies this paper at http://www.nature.com/naturecommunications

Competing financial interests: The authors declare no competing financial interests.

Reprints and permission information is available online at http://npg.nature.com/reprintsandpermissions/

How to cite this article: Asmara, T. C. *et al.* Mechanisms of charge transfer and redistribution in $LaAlO_3/SrTiO_3$ revealed by high-energy optical conductivity. *Nat. Commun.* 5:3663 doi: 10.1038/ncomms4663 (2014).